

# High-fidelity and robust two-qubit gates for quantum-dot spin qubits in silicon

Chia-Hsien Huang,<sup>1,2</sup> C. H. Yang,<sup>3</sup> Chien-Chang Chen,<sup>1,2</sup> A. S. Dzurak,<sup>3</sup> and Hsi-Sheng Goan<sup>1,2,\*</sup>

<sup>1</sup>*Department of Physics and Center for Theoretical Physics,  
National Taiwan University, Taipei 10617, Taiwan*

<sup>2</sup>*Center for Quantum Science and Engineering, National Taiwan University, Taipei 10617, Taiwan*

<sup>3</sup>*Centre for Quantum Computation and Communication Technology,  
School of Electrical Engineering and Telecommunications,  
The University of New South Wales, Sydney, New South Wales 2052, Australia*

(Dated: March 16, 2022)

A two-qubit controlled-NOT (CNOT) gate, realized by a controlled-phase (C-phase) gate combined with single-qubit gates, has been experimentally implemented recently for quantum-dot spin qubits in isotopically enriched silicon, a promising solid-state system for practical quantum computation. In the experiments, the single-qubit gates have been demonstrated with fault-tolerant control-fidelity, but the infidelity of the two-qubit C-phase gate is, primarily due to the electrical noise, still higher than the required error threshold for fault-tolerant quantum computation (FTQC). Here, by taking the realistic system parameters and the experimental constraints on the control pulses into account, we construct experimentally realizable high-fidelity CNOT gates robust against electrical noise with the experimentally measured  $1/f^{1.01}$  noise spectrum and also against the uncertainty in the interdot tunnel coupling amplitude. Our optimal CNOT gate has about two orders of magnitude improvement in gate infidelity over the ideal C-phase gate constructed without considering any noise effect. Furthermore, within the same control framework, high-fidelity and robust single-qubit gates can also be constructed, paving the way for large-scale FTQC.

PACS numbers: 03.67.Lx, 03.67.Pp, 03.67.-a, 73.21.La

Electron spin qubits in semiconductor quantum dots [1] are promising solid-state systems to realize quantum computation. Significant progresses of quantum-dot spin qubits for quantum information processing have been made with III-V semiconductors such as GaAs [2–14], but the coherence time of the qubits is limited by the strong dephasing from the environment nuclear spins [15]. On the other hand, the coherence time is substantially improved by using a Si-based host substrate [16–25]. For qubits in isotopically enriched  $^{28}\text{Si}$ , the decoherence (dephasing) time  $T_2^*$  can be further extended to  $120\mu\text{s}$  [18, 19]. So far, the single-qubit gates for silicon-based quantum-dot spin-qubit systems have been demonstrated with fault-tolerant control-fidelity [18, 19, 21, 23, 24]. The two-qubit gates have also been realized [19, 24, 25], but their fidelities have not yet reached the criterion for fault-tolerant quantum computation (FTQC), primarily due to the noise of the electrical voltage control used to realize the two-qubit gate. Some theoretical pulse-design schemes to improve fidelity for two-qubit gates have been proposed [26, 27].

The goal of this paper is to construct experimentally realizable robust two-qubit gates for quantum-dot spin qubits in isotopically enriched silicon with fidelity enabling large-scale FTQC. To this end, we apply a robust control method [28] to suppress the electrical noise with the experimentally measured  $1/f^{1.01}$  noise spectrum [23] using the realistic system parameters [19]. The experimental constraint on the maximum ac magnetic field strength due to the power limitation through the on-chip electron spin resonance (ESR) line and the filtering ef-

fects on the control pulses due to the finite bandwidth of waveform generators are also accounted for. Due to the expected long coherence time in isotopically enriched silicon system, we do not consider the single-qubit decoherence (dephasing) noise in our calculations as it does not affect appreciably the performance of the gates we construct [29]. Instead of decomposing a CNOT gate into a C-phase gate and several single-qubit gates in series as in the experiment [19], we can construct single smooth pulses for the high-fidelity CNOT gates directly to reduce the gate operation time and the accumulated gate errors from the decomposed gates. Compared with the ideal C-phase gate constructed without considering any noise, our optimal CNOT gate can improve the fidelity loss from the electrical noise by near two orders of magnitude (fidelity=99.997%) and enlarge the robust window against the uncertainty of the system parameter by about 10 times. Besides, our smooth pulses with zero strength and zero derivative at the initial and final gate operation times can avoid the fidelity-loss due to the rise time and fall time issues between the pulse-pulse connections of adjacent gate operations. We also investigate other possible  $1/f^\alpha$  noise spectra with  $0.7 \leq \alpha < 1.01$ , and demonstrate that for the case of  $\alpha = 0.7$ , the infidelity of the high-fidelity CNOT gates by the same control method [28] under the same experimental constraints can still have one order of magnitude improvement over the ideal C-phase gate.

In our scheme, the detuning energy is kept to a constant value when operating a sequence of single-qubit and two-qubit gates. In contrast, in the experiment [19], a

single-qubit gate is realized by tuning down the detuning energy (or relative alignment potential of the two dots) to a small constant value as compared to the on-site double-occupancy Coulomb energy to decouple the two-qubit coupling; inversely, a two-qubit gate is realized by tuning up the detuning energy to a large constant value to increase the coupling between the two qubits. However, when operating a sequence of single-qubit gates and two-qubit gates, the rise and fall times of the detuning energy between two-qubit gate and single-qubit gates would cause gate errors. Besides, changing detuning energy accompanies stark shifts on the quantum-dot qubits, which may result in additional gate errors if the calibration is not precise. Therefore, to prevent the fidelity degradation from tuning the detuning energy up and down, we propose to operate a sequence of single-qubit and two-qubit gates with the detuning energy fixed.

In the following, we first introduce the ideal system of the quantum-dot spin qubits in isotopically enriched silicon [19], then analyze the factors that degrade the gate fidelity in a realistic system, after that briefly introduce the robust control method [28], and finally demonstrate the performance of high-fidelity and robust CNOT and single-qubit gates in the same control framework, i.e., with detuning energy fixed and ac magnetic field as the control field.

For the quantum-dot electron spin qubits in isotopically enriched silicon, the ideal two-qubit Hamiltonian written in the basis states of  $(|\text{dot2}, \text{dot1}\rangle =) |\uparrow, \uparrow\rangle, |\uparrow, \downarrow\rangle, |\downarrow, \uparrow\rangle, |\downarrow, \downarrow\rangle$  and  $|0, 2\rangle$  can be expressed as

$$\mathcal{H}_I(t)/h = \begin{pmatrix} \bar{E}_Z & \frac{1}{2}E_X(t) & \frac{(1+\eta)}{2}E_X(t) & 0 & 0 \\ \frac{1}{2}E_X(t) & \frac{1}{2}\delta E_Z & 0 & \frac{(1+\eta)}{2}E_X(t) & t_0 \\ \frac{(1+\eta)}{2}E_X(t) & 0 & -\frac{1}{2}\delta E_Z & \frac{1}{2}E_X(t) & -t_0 \\ 0 & \frac{(1+\eta)}{2}E_X(t) & \frac{1}{2}E_X(t) & -\bar{E}_Z & 0 \\ 0 & t_0 & -t_0 & 0 & U - \epsilon(t) \end{pmatrix}, \quad (1)$$

where  $h$  is the Plank constant,  $\bar{E}_Z = (E_{Z_1} + E_{Z_2})/2$  is the average frequency and  $\delta E_Z = (E_{Z_2} - E_{Z_1})$  is the frequency difference of Zeeman splitting in the  $z$ -direction for dot1 and dot2,  $E_{Z_1}$  and  $E_{Z_2}$ , respectively,  $t_0$  is the interdot tunnel coupling and  $hU$  is the on-site Coulomb energy, and  $h\epsilon$  is the detuning energy or relative alignment of the potential of the two dots. In principle, Zeeman splitting frequency in the  $x$ -direction for dot1 and dot2 can be different and denoted as  $E_X(t)$  and  $(1+\eta)E_X(t)$ , respectively, where  $E_X(t) = g\mu_B B_X(t)/h$ . Here  $\eta$  is the  $x$ -direction  $g$  factor difference fraction between two dots, and the corresponding value for the  $z$ -direction is  $\sim 0.001$  in the experiment [19]. Without losing generality, we choose  $\eta = 0$  to demonstrate the gate performance here. We have examined the controllability of  $\mathcal{H}_I(t)$  of Eq. (1) for CNOT gates and single-qubit gates, and the same level of performance as  $\eta = 0$  case can be

achieved for  $|\eta| \leq 0.1$  cases. We control ac magnetic field  $B_X(t) = \Omega_X(t) \cos(\bar{E}_Z 2\pi t) + \Omega_Y(t) \cos(\bar{E}_Z 2\pi t + \frac{\pi}{2})$  via an on-chip ESR line with amplitudes  $\Omega_X(t)$  and  $\Omega_Y(t)$  to operate quantum gates. In the experiment [19], the C-phase gate is realized by tuning the detuning energy  $\epsilon$  to a constant value [with the ac magnetic field  $B_X(t)$  off] to accumulate the time-integrated phase shift via the effective detuning frequency  $\nu_{\uparrow\downarrow, (\downarrow\uparrow)}$ . There, the system parameters  $\bar{E}_Z = 39.16\text{GHz}$ ,  $\delta E_Z = -40\text{MHz}$ , and  $t_0 = 900\text{MHz}$ . We will use also these realistic system parameters to construct high-fidelity and robust CNOT gates and single-qubit gates demonstrated later.

We define the ideal gate infidelity as  $J_1 \equiv 1 - |\text{Tr}[U_T^\dagger U_{I,4\times 4}(t_f)]|^2/16$ , where  $\text{Tr}$  denotes a trace over the 2-qubit system state space,  $U_T$  is the two-qubit target gate, and  $U_{I,4\times 4}(t_f)$  is the projected propagator in the subspace spanned by the two-qubit computational basis states  $\{|\uparrow, \uparrow\rangle, |\uparrow, \downarrow\rangle, |\downarrow, \uparrow\rangle, |\downarrow, \downarrow\rangle\}$  obtained from the ideal system propagator  $U_I(t_f) = \mathcal{T}_+ \exp\left[-(i/\hbar) \int_0^{t_f} \mathcal{H}_I(t') dt'\right]$  at the final gate operation time  $t_f$ , where  $\mathcal{T}_+$  is the time-ordering operator. In the definition of the ideal gate infidelity  $J_1$ , the leakage error, i.e., the state probability remains in the  $|0, 2\rangle$  subspace, is also accounted for.

However, in a realistic system, there exist many factors degrading the gate fidelity such as the electrical noise  $\beta_{U-\epsilon}(t)$ , the uncertainty  $\alpha_{t_0}$  in tunnel coupling  $t_0$ , and the filtering effects on the control pulses due to the finite bandwidth of waveform generators. So, a realistic Hamiltonian taking these factors into account becomes

$$\mathcal{H}(t)/h = \begin{pmatrix} \bar{E}_Z & \frac{1}{2}E_X^{\text{filt}}(t) & \frac{1}{2}E_X^{\text{filt}}(t) & 0 & 0 \\ \frac{1}{2}E_X^{\text{filt}}(t) & \frac{1}{2}\delta E_Z & 0 & \frac{1}{2}E_X^{\text{filt}}(t) & (t_0 + \alpha_{t_0}) \\ \frac{1}{2}E_X^{\text{filt}}(t) & 0 & -\frac{1}{2}\delta E_Z & \frac{1}{2}E_X^{\text{filt}}(t) & -(t_0 + \alpha_{t_0}) \\ 0 & \frac{1}{2}E_X^{\text{filt}}(t) & \frac{1}{2}E_X^{\text{filt}}(t) & -\bar{E}_Z & 0 \\ 0 & (t_0 + \alpha_{t_0}) & -(t_0 + \alpha_{t_0}) & 0 & U - \epsilon + \beta_{U-\epsilon}(t) \end{pmatrix}, \quad (2)$$

where  $E_X^{\text{filt}}(t) = (g\mu_B/h)[\Omega_X^{\text{filt}}(t) \cos(\bar{E}_Z 2\pi t) + \Omega_Y^{\text{filt}}(t) \cos(\bar{E}_Z 2\pi t + \frac{\pi}{2})]$  with  $\Omega_X^{\text{filt}}(t)$  and  $\Omega_Y^{\text{filt}}(t)$  being the actual output control pulses on the qubits with the filtering effects accounted for. We assume the electrical noise  $\beta_{U-\epsilon}(t)$  is accompanied by the electrical control of the detuning energy  $\epsilon$  and appears in the same location of  $\epsilon$  in the Hamiltonian. The value of the interdot tunnel coupling  $t_0$  is obtained by fitting the experimental data, and thus there may exist some uncertainty  $\alpha_{t_0}$  for  $t_0$  extraction. We regard  $\alpha_{t_0}$  as a systematic error, that is  $\alpha_{t_0}$  is a fixed constant value for a specific two-qubit system, but the fixed constant  $\alpha_{t_0}$  can vary for different two-qubit systems. Therefore, a more realistic gate infidelity should be defined as

$$\mathcal{I} \equiv 1 - \frac{1}{16} \left| \text{Tr} \left[ U_T^\dagger U_{4\times 4}(t_f) \right] \right|^2, \quad (3)$$

where  $U_{4 \times 4}(t_f)$  is the realistic propagator in the subspace spanned by the two-qubit computational basis states, projected from the realistic propagator  $U(t_f) = \mathcal{T}_+ \exp[-(i/\hbar) \int_0^{t_f} \mathcal{H}(t') dt']$  at  $t_f$ . In general, noise is stochastic, and thus we denote the ensemble average of gate infidelity  $\mathcal{I}$  over the different noise realizations as  $\langle \mathcal{I} \rangle$ .

To characterize the electrical noise  $\beta_{U-\epsilon}(t)$ , we simulate the two-qubit dephasing process, the free induction evolution of the two-qubit system, as shown in Fig. 1(a) or more precisely in Fig. S6 of the Supplementary Information of Ref. [19]. There, the probability of the state  $|\uparrow, \downarrow\rangle$ ,  $P(|\uparrow, \downarrow\rangle)$  (the spin up fraction of dot2 in the  $|\text{dot2}, \text{dot1}\rangle$  basis), for initial state  $|\downarrow, \downarrow\rangle$  after the operations  $(\pi/2)_{X_2} \rightarrow \text{C-phase}(\tau_Z) \rightarrow (\pi/2)_{Y_2}$  with increasing time  $\tau_Z$  (gate operation time of C-phase gate) is measured. It was mentioned in the caption of Fig. S6 of Ref. [19] that there exists a phase difference  $\phi = \pi/2$  separated by the C-phase( $\tau_Z$ ) gate, for which we simulate by inserting a  $(\pi/2)_{Z_2}$  rotation between the  $(\pi/2)_{X_2}$  rotation and the C-phase( $\tau_Z$ ) gate. Here gates  $(\pi/2)_{X_2}$ ,  $(\pi/2)_{Y_2}$ , and  $(\pi/2)_{Z_2}$  represent  $\pi/2$  rotations in the  $X$ -direction,  $Y$ -direction, and  $Z$ -direction, respectively, for the dot2 qubit. To estimate the strength of the electrical noise causing the two-qubit dephasing effect shown in Fig. S6 of Ref. [19], we assume that all single-qubit rotations (gates) are ideal, and thus the probability loss in Fig. S6 of Ref. [19] comes entirely from the C-phase gate suffering from the electrical noise. We model the electrical noise  $\beta_{U-\epsilon}(t)$  in the isotope-enriched silicon QD system having the same experimentally measured  $1/f^{1.01}$  noise spectrum as that in isotope-enriched  $^{28}\text{Si}/\text{SiGe}$  quantum dots [23] in the frequency range between  $\omega/2\pi = 10^{-2}\text{Hz}$  and  $10^6\text{Hz}$ . To avoid the divergence of  $1/f^{1.01}$  noise spectrum at very low frequency, we assume the noise spectrum  $S(\omega)$  gradually saturates to a constant value for frequency  $\omega/2\pi < 10^{-2}\text{Hz}$ . This  $1/f^{1.01}$  noise spectrum can be simulated via a superposition of Ornstein-Uhlenbeck processes [30, 31]. For the C-phase gate reported in the experiment of Fig. S6 of Ref. [19], the effective detuning frequency  $\nu_{\uparrow\downarrow} = 3.14\text{MHz}$  corresponds to  $U - \epsilon = 276.71\text{GHz}$  that can be tuned by the electrical voltage. Employing the Hamiltonian  $\mathcal{H}(t)$  of Eq. (2) with these realistic system parameters, we simulate the ensemble average probability  $\langle P(|\uparrow, \downarrow\rangle) \rangle$  with increasing time  $\tau_Z$  for different values of average standard deviation  $\sigma_{U-\epsilon}$  of the electrical noise, each using a thousand of  $\beta_{U-\epsilon}(t)$  noise realizations. We observe that when  $\sigma_{U-\epsilon}$  is chosen to be  $2.4\text{GHz}$ , the corresponding two-qubit coherence (dephasing) time  $T_{2,CZ}^* = 8.57\mu\text{s}$  is obtained by fitting the ensemble average probability  $\langle P(|\uparrow, \downarrow\rangle) \rangle$  with increasing time  $\tau_Z$  to the formula  $\frac{1}{2} + \frac{1}{2} \cos(2\pi \cdot f_{2,CZ} \cdot \tau_Z) \cdot \exp[-(\tau_Z/T_{2,CZ}^*)^a]$  [23], where we choose  $f_{2,CZ} = \nu_{\uparrow\downarrow} = 3.14\text{MHz}$  and  $a = 1.9$  for the best fitting result. The simulation data points (in blue) and the best fitting curve (in red) of  $\langle P(|\uparrow, \downarrow\rangle) \rangle$  are shown

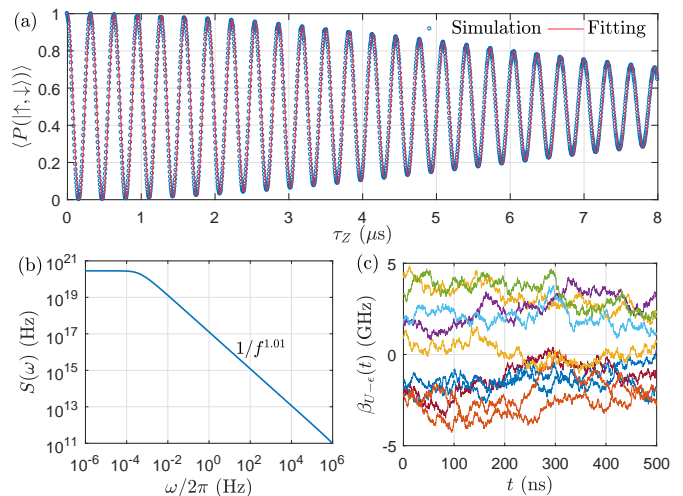


FIG. 1. Characterization of the electrical noise  $\beta_{U-\epsilon}(t)$ . (a) The ensemble average probability  $\langle P(|\uparrow, \downarrow\rangle) \rangle$  suffering the electrical noise  $\beta_{U-\epsilon}(t)$  with the standard deviation  $\sigma_{U-\epsilon} = 2.4\text{GHz}$  is simulated in the blue circles and fitted in the red line. (b) The corresponding spectrum  $S(\omega)$  of the electrical noise  $\beta_{U-\epsilon}(t)$  with  $1/f^{1.01}$  property from  $\omega/2\pi = 10^{-2}$  to  $10^6$ . (c) Ten realizations of the corresponding electrical noise  $\beta_{U-\epsilon}(t)$ .

in Fig. 1(a), and the corresponding noise spectrum  $S(\omega)$  and typical noise realizations  $\beta_{U-\epsilon}(t)$  are shown in Figs. 1(b) and 1(c), respectively. This result is very close to the experimentally measured  $T_{2,CZ}^* = 8.3\mu\text{s}$  [19]. Therefore, we use the electrical noise  $\beta_{U-\epsilon}(t)$  with noise spectrum  $1/f^{1.01}$  and average standard deviation  $\sigma_{U-\epsilon} = 2.4\text{GHz}$  and choose  $U - \epsilon = 276.71\text{GHz}$  for the following quantum gate simulations.

To suppress the  $1/f^{1.01}$  electrical noise we characterize above, we employ the robust control method [28] to minimize the total cost function

$$\mathcal{K}[\Omega_X(t), \Omega_Y(t)] = J_1 + \langle J_{2,U-\epsilon} \rangle + \xi \mathcal{F} \quad (4)$$

via searching the optimal control parameter sets  $\{a_1, a_2, \dots, a_{k_{\max}}\}$  and  $\{b_1, b_2, \dots, b_{k_{\max}}\}$  in the respective control pulses  $\Omega_X(t) = \sum_{k=1}^{k_{\max}} a_k \sin^3(\omega_{X,k} t)$  and  $\Omega_Y(t) = \sum_{k=1}^{k_{\max}} b_k \sin^3(\omega_{Y,k} t)$  where we choose  $\omega_{X,k} = (2k-1)\pi/t_f$  and  $\omega_{Y,k} = (2k)\pi/t_f$ , and choose  $k_{\max} = 11$  for CNOT gates and  $k_{\max} = 8$  for single-qubit gates. The function form of  $\sin^3(\omega_{X/Y,k} t)$  in the control pulses  $\Omega_X(t)$  and  $\Omega_Y(t)$  is chosen to make pulse strengths and pulse slopes vanish at both  $t = 0$  and  $t = t_f$  for smooth pulse-pulse connection to avoid the extra fidelity loss from the sudden pulse strength change when connecting to their previous or subsequent gate operations. In the total cost function  $\mathcal{K}$  in Eq. (4),  $J_1$  is the ideal gate infidelity, and  $\langle J_{2,U-\epsilon} \rangle = \frac{1}{2} \int_0^{t_f} 2\pi dt_1 \int_0^{t_1} 2\pi dt_2 C_{U-\epsilon}(t_1, t_2) \times \text{Re}\{\text{Tr}[(R_{U-\epsilon}(t_1)R_{U-\epsilon}(t_2))_{4 \times 4}]\} - \frac{1}{16} \int_0^{t_f} 2\pi dt_1 \int_0^{t_f} 2\pi dt_2$

$C_{U-\epsilon}(t_1, t_2) \text{Tr}[R_{U-\epsilon, 4 \times 4}(t_1)] \text{Tr}[R_{U-\epsilon, 4 \times 4}(t_2)]$  is the lowest order contribution from the electrical noise  $\beta_{U-\epsilon}(t)$  in the ensemble average infidelity  $\langle \mathcal{I} \rangle$ , where  $C_{U-\epsilon}(t_1, t_2) = \langle \beta_{U-\epsilon}(t_1) \beta_{U-\epsilon}(t_2) \rangle$  is the correlation function of the electrical noise and can be obtained from the noise spectrum  $S(\omega)$  in Fig. 1(b) via the Wiener-Khinchin theorem, i.e.,  $C_{U-\epsilon}(t_1, t_2) = C_{U-\epsilon}(t_1 - t_2) = \frac{1}{2\pi} \int_{-\infty}^{\infty} S(\omega) e^{i\omega(t_1 - t_2)} d\omega$  [32]. The operators  $[R_{U-\epsilon}(t_1) R_{U-\epsilon}(t_2)]_{4 \times 4}$  and  $R_{U-\epsilon, 4 \times 4}(t)$  are  $R_{U-\epsilon}(t_1) R_{U-\epsilon}(t_2)$  and  $R_{U-\epsilon}(t)$  projected onto the subspace spanned by the computational basis states, respectively. Here  $R_{U-\epsilon}(t) \equiv U_I^\dagger(t) H_{U-\epsilon} U_I(t)$ ,  $U_I(t)$  is the ideal propagator obtained by the ideal Hamiltonian  $\mathcal{H}_I(t)$  in Eq. (1), and  $H_{U-\epsilon}$  is a  $5 \times 5$  matrix of the electrical noise Hamiltonian with all matrix elements being zeros except one element with value being one in the location of  $U - \epsilon(t)$  in Eq. (1), i.e.,  $H_{U-\epsilon}(5, 5) = 1$ . The quantity  $\mathcal{F}$  in the last term of Eq. (4) defined as  $\mathcal{F} \equiv \int_0^{t_f} |\Omega_X(t)|^2 dt + \int_0^{t_f} |\Omega_Y(t)|^2 dt + \left| \int_0^{t_f} |\Omega_X(t)|^2 dt - \int_0^{t_f} |\Omega_Y(t)|^2 dt \right|$  is the fluence (a measure of the field energy) [33], which is used to restrain or minimize the strengths of ac magnetic field control pulses  $\Omega_X(t)$  and  $\Omega_Y(t)$ . The factor  $\xi$  also in the same last term of Eq. (4) determines the contribution ratio of the fluence  $\mathcal{F}$  to the ensemble average infidelity in the total cost function. If  $\xi$  is too small,  $\mathcal{F}$  does not work. However, if  $\xi$  is too large, then  $\mathcal{F}$  dominates the contribution in the cost function and thus  $\langle J_{2, U-\epsilon} \rangle$  may not be effectively suppressed. In our simulations, we find  $\xi = 10^{-6}$  works effectively.

To meet the constraint of maximum pulse strength 1mT, we suitably choose the gate operation time  $t_f = 500\text{ns}$  for CNOT gates and  $t_f = 200\text{ns}$  and  $250\text{ns}$  for single-qubit  $I_2 \otimes X_1$  gate (Identity gate for dot2 qubit and  $X$  gate for dot1 qubit) and  $H_2 \otimes I_1$  gate (Hadamard gate for dot2 qubit and Identity gate for dot1 qubit), respectively. After running the optimization procedure, we obtain the optimal gate pulses that can suppress the electrical noise while keeping the maximum strength of the optimal ac magnetic field control pulses smaller than 1mT. However, due to the finite bandwidth of waveform generators the actual output pulses  $\Omega_X^{\text{filt}}(t)$  and  $\Omega_Y^{\text{filt}}(t)$  on the qubits will be distorted as compared to the input optimal pulses  $\Omega_X(t)$  and  $\Omega_Y(t)$ . The filtering effects of the waveform generators can be modeled via the transfer function  $\Omega^{\text{filt}}(t) = \frac{1}{2\pi} \int_{-\infty}^{+\infty} d\omega e^{i\omega t} F(\omega) \Omega(\omega)$ , where  $\Omega(\omega) = \int_{-\infty}^{+\infty} dt' e^{-i\omega t'} \Omega(t')$  is the input optimal pulse in the frequency domain, and  $F(\omega) = \exp(-\omega^2/\omega_c^2)$  is the response function of the filter with  $\omega_c$  being the cutoff frequency [34, 35]. We use the value of  $\omega_c/2\pi = 425.4\text{MHz}$  (approximation for Tektronix AWG5014 [34, 35]) for simulating the filtering effects on the quantum gates demonstrated here. The pulse distortion due to the filtering effects will degrade the gate fidelity from the expected value. Thus, we perform an extra fine-tuning optimization

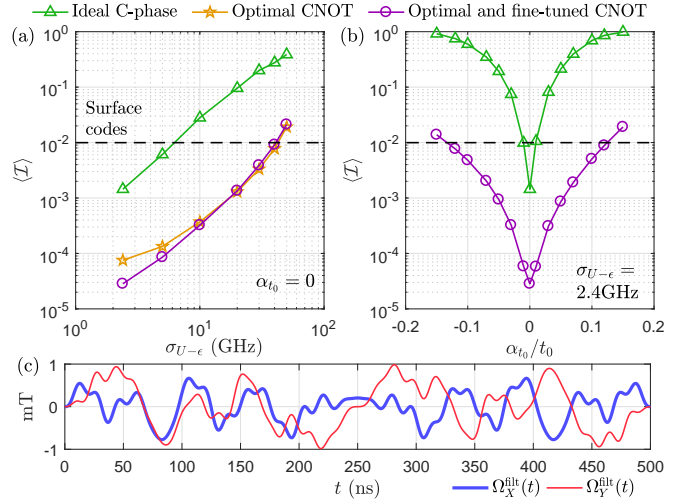


FIG. 2. The robust performance (a) against the electrical noise  $\beta_{U-\epsilon}(t)$  with  $1/f^{1.01}$  noise spectrum and (b) against the uncertainty  $\alpha_{t_0}$  in  $t_0$  under  $\sigma_{U-\epsilon} = 2.4\text{GHz}$  for the ideal C-phase gate in the green-triangle line, the optimal CNOT gate without fine-tuning optimization in the orange-pentagram line, and the optimal CNOT gate with fine-tuning optimization in the purple-circle line. (c) The actual output pulses with the filtering effects,  $\Omega_X^{\text{filt}}(t)$  in bold-blue line and  $\Omega_Y^{\text{filt}}(t)$  in thin-red line, for the optimal and fine-tuned CNOT gate.

with the same cost function  $\mathcal{K}$  in Eq. (4) but replacing the unfiltered pulses  $\Omega_X(t)$  and  $\Omega_Y(t)$  with the filtered pulses  $\Omega_X^{\text{filt}}(t)$  and  $\Omega_Y^{\text{filt}}(t)$  to obtain the fine-tuned optimal gate pulses to recover the fidelity loss. For computation efficiency [29], we calculate the total cost function  $\mathcal{K}$  in Eq. (4) to obtain the optimal control pulses using an effective Hamiltonian with the rotating-wave approximation and the second-order approximation after the Schrieffer-Wolff transformation [36], while we use the full realistic Hamiltonian  $\mathcal{H}(t)$  of Eq. (2) without these approximations to simulate the ensemble average infidelity  $\langle \mathcal{I} \rangle$  with an ensemble of one thousand noise realizations for demonstrating the gate performance.

The robust performance against the electrical noise  $\beta_{U-\epsilon}(t)$  with  $1/f^{1.01}$  noise spectrum is shown in Fig. 2(a). The optimal CNOT gate with the fine-tuning optimization in the purple-circle line can recover the degradation in the ensemble average infidelity  $\langle \mathcal{I} \rangle$  resulting from the filtering effects (in the orange-pentagram line) by about half-order of magnitude for smaller  $\sigma_{U-\epsilon}$ . For larger  $\sigma_{U-\epsilon}$ , the contribution of infidelity increase due to the filtering effect is much smaller than that due to the electrical noise so that no considerable improvement is observed. However, the fine-tuned optimal CNOT gate can improve the ensemble average infidelity  $\langle \mathcal{I} \rangle$  over the ideal C-phase gate in the green-triangle line by near two orders of magnitude at  $\sigma_{U-\epsilon} = 2.4\text{GHz}$ , and for gate error (infidelity) less than the error threshold of surface codes  $\langle \mathcal{I} \rangle \lesssim 10^{-2}$  [37], the fine-tuned optimal

CNOT gate can be robust against the noise strength to  $\sigma_{U-\epsilon} \cong 40\text{GHz}$  while the ideal C-phase gate can be robust only to  $\sigma_{U-\epsilon} \cong 6\text{GHz}$ . The uncertainty error  $\alpha_{t_0}$  in tunnel coupling  $t_0$  appears in the same location as  $\beta_{U-\epsilon}(t)$  in the effective Hamiltonian after the Schrieffer-Wolff transformation [36], and thus the constructed optimal gate pulses robust against the electrical noise will be also robust against the uncertainty error  $\alpha_{t_0}$  in  $t_0$ . This can be seen in Fig. 2(b) that our fine-tuned optimal CNOT gate at the electrical noise  $\sigma_{U-\epsilon} = 2.4\text{GHz}$  can be robust against uncertainty  $\alpha_{t_0}$  to about 12% of  $t_0$  (in the purple-circle line), while the ideal C-phase gate can be robust against  $\alpha_{t_0}$  to only about 1% of  $t_0$  (in the green-triangle line) for  $\langle \mathcal{I} \rangle \lesssim 10^{-2}$ . The actual output pulses on the qubits with the filtering effects of the fine-tuned optimal CNOT gate in Figs. 2(a) and 2(b) are shown in Fig. 2(c), and the maximum strengths of  $|\Omega_X^{\text{filt}}(t)|$  and  $|\Omega_Y^{\text{filt}}(t)|$  within the gate operation time  $t_f = 500\text{ns}$  are all smaller than 1mT. Under the same experimental constraints, control framework, and voltage setting as the two-qubit CNOT gate in Fig. 2, high-fidelity and robust single-qubit gates can also be realized. For example, we find that our optimal  $I_2 \otimes X_1$  and  $H_2 \otimes I_1$  gates with the fine-tuning optimization can be robust against the electrical noise to  $\sigma_{U-\epsilon} \cong 50\text{GHz}$  for  $\langle \mathcal{I} \rangle \lesssim 10^{-2}$ , and at  $\sigma_{U-\epsilon} = 2.4\text{GHz}$  the gate infidelity  $\langle \mathcal{I} \rangle \cong 2 \times 10^{-5}$ . We also investigate the performance of the CNOT gate for  $1/f^\alpha$  electrical noise spectra with  $0.7 \leq \alpha < 1.01$ , which have larger high-frequency contributions than the  $1/f^{1.01}$  noise spectrum. As  $\alpha$  decreases from 1.01 to 0.7, the  $\langle \mathcal{I} \rangle$  of the fine-tuned optimal CNOT gate constructed via the same robust control method [28] gradually increases from  $2.84 \times 10^{-5}$  to  $2.5 \times 10^{-4}$ , but still having improvement from two-order to one-order over the ideal C-phase gate.

In summary, we have constructed a high-fidelity CNOT gate and single-qubit gates robust against the time-varying electrical noise  $\beta_{U-\epsilon}(t)$  with the experimentally measured  $1/f^{1.01}$  noise spectrum and against the system parameter uncertainty  $\alpha_{t_0}$  in  $t_0$ . In our proposed control framework, the detuning  $\epsilon$  is kept constant for all single- and two-qubit gate operations to avoid possible extra errors coming from tuning  $\epsilon$  up and down for a sequence of gate operations. We control only two experimentally realizable ac magnetic fields with pulse strengths satisfying the constraint of the device. Our scheme that can also recover the fidelity loss from the filtering effects will provide an essential step toward large-scale FTQC for quantum-dot spin qubits in isotopically enriched silicon.

We acknowledge support from the the Ministry of Science and Technology of Taiwan under Grant No. MOST 106-2112-M-002-013-MY3, from the National Taiwan University under Grant No. NTU-CCP-106R891703, and from the thematic group program of the National Center for Theoretical Sciences, Taiwan. C.H.Y. and A.S.D. acknowledge support from the Australian Research Council (CE11E0001017) and the US Army Research Office

(W911NF-17-1-0198).

- 
- \* goan@phys.ntu.edu.tw
- [1] D. Loss and D. P. DiVincenzo, Phys. Rev. A **57**, 120 (1998).
  - [2] J. R. Petta, A. C. Johnson, J. M. Taylor, E. A. Laird, A. Yacoby, M. D. Lukin, C. M. Marcus, M. P. Hanson, and A. C. Gossard, Science **309**, 2180 (2005).
  - [3] F. H. L. Koppens, C. Buizert, K. J. Tielrooij, I. T. Vink, K. C. Nowack, T. Meunier, L. P. Kouwenhoven, and L. M. K. Vandersypen, Nature **442**, 766 (2006).
  - [4] F. H. L. Koppens, K. C. Nowack, and L. M. K. Vandersypen, Phys. Rev. Lett. **100**, 236802 (2008).
  - [5] D. J. Reilly, J. M. Taylor, J. R. Petta, C. M. Marcus, M. P. Hanson, and A. C. Gossard, Science **321**, 817 (2008).
  - [6] S. Foletti, H. Bluhm, D. Mahalu, V. Umansky, and A. Yacoby, Nat. Phys. **5**, 903 (2009).
  - [7] H. Bluhm, S. Foletti, D. Mahalu, V. Umansky, and A. Yacoby, Phys. Rev. Lett. **105**, 216803 (2010).
  - [8] C. Barthel, J. Medford, C. M. Marcus, M. P. Hanson, and A. C. Gossard, Phys. Rev. Lett. **105**, 266808 (2010).
  - [9] H. Bluhm, S. Foletti, I. Neder, M. Rudner, D. Mahalu, V. Umansky, and A. Yacoby, Nat. Phys. **7**, 109 (2011).
  - [10] K. C. Nowack, M. Shafiei, M. Laforest, G. E. D. K. Prawiroatmodjo, L. R. Schreiber, C. Reichl, W. Wegscheider, and L. M. K. Vandersypen, Science **333**, 1269 (2011).
  - [11] R. Brunner, Y.-S. Shin, T. Obata, M. Pioro-Ladrière, T. Kubo, K. Yoshida, T. Taniyama, Y. Tokura, and S. Tarucha, Phys. Rev. Lett. **107**, 146801 (2011).
  - [12] M. D. Shulman, O. E. Dial, S. P. Harvey, H. Bluhm, V. Umansky, and A. Yacoby, Science **336**, 202 (2012).
  - [13] J. Medford, J. Beil, J. M. Taylor, S. D. Bartlett, A. C. Doherty, E. I. Rashba, D. P. DiVincenzo, H. Lu, A. C. Gossard, and C. M. Marcus, Nat. Nanotech. **8**, 654 (2013).
  - [14] J. M. Nichol, L. A. Orona, S. P. Harvey, S. Fallahi, G. C. Gardner, M. J. Manfra, and A. Yacoby, npj Quantum Information **3**, 3 (2017).
  - [15] E. A. Chekhovich, M. N. Makhonin, A. I. Tartakovskii, A. Yacoby, H. Bluhm, K. C. Nowack, and L. M. K. Vandersypen, Nat. Mater. **12**, 494 (2013).
  - [16] B. M. Maune, M. G. Borselli, B. Huang, T. D. Ladd, P. W. Deelman, K. S. Holabird, A. A. Kiselev, I. Alvarado-Rodriguez, R. S. Ross, A. E. Schmitz, M. Sokolich, C. A. Watson, M. F. Gyure, and A. T. Hunter, Nature **481**, 344 (2012).
  - [17] E. Kawakami, P. Scarlino, D. R. Ward, F. R. Braakman, D. E. Savage, M. G. Lagally, M. Friesen, S. N. Coppersmith, M. A. Eriksson, and L. M. K. Vandersypen, Nat. Nanotech. **9**, 666 (2014).
  - [18] M. Veldhorst, J. C. C. Hwang, C. H. Yang, A. W. Leenstra, B. de Ronde, J. P. Dehollain, J. T. Muhonen, F. E. Hudson, K. M. Itoh, A. Morello, and A. S. Dzurak, Nat. Nanotech. **9**, 981 (2014).
  - [19] M. Veldhorst, C. H. Yang, J. C. C. Hwang, W. Huang, J. P. Dehollain, J. T. Muhonen, S. Simmons, A. Laucht, F. E. Hudson, K. M. Itoh, A. Morello, and A. S. Dzurak, Nature **526**, 410 (2015).

- [20] K. Eng, T. D. Ladd, A. Smith, M. G. Borselli, A. A. Kiselev, B. H. Fong, K. S. Holabird, T. M. Hazard, B. Huang, P. W. Deelman, I. Milosavljevic, A. E. Schmitz, R. S. Ross, M. F. Gyure, and A. T. Hunter, *Science Advances* **1** (2015), 10.1126/sciadv.1500214.
- [21] K. Takeda, J. Kamioka, T. Otsuka, J. Yoneda, T. Nakajima, M. R. Delbecq, S. Amaha, G. Allison, T. Kodera, S. Oda, and S. Tarucha, *Science Advances* **2** (2016), 10.1126/sciadv.1600694.
- [22] E. Kawakami, T. Jullien, P. Scarlino, D. R. Ward, D. E. Savage, M. G. Lagally, V. V. Dobrovitski, M. Friesen, S. N. Coppersmith, M. A. Eriksson, and L. M. K. Vandersypen, *Proceedings of the National Academy of Sciences* **113**, 11738 (2016).
- [23] J. Yoneda, K. Takeda, T. Otsuka, T. Nakajima, M. R. Delbecq, G. Allison, T. Honda, T. Kodera, S. Oda, Y. Hoshi, N. Usami, K. M. Itoh, and S. Tarucha, *Nature Nanotechnology* **13**, 102 (2018).
- [24] D. M. Zajac, A. J. Sigillito, M. Russ, F. Borjans, J. M. Taylor, G. Burkard, and J. R. Petta, *Science* **359**, 439 (2018).
- [25] T. F. Watson, S. G. J. Philips, E. Kawakami, D. R. Ward, P. Scarlino, M. Veldhorst, D. E. Savage, M. G. Lagally, M. Friesen, S. N. Coppersmith, M. A. Eriksson, and L. M. K. Vandersypen, *Nature* (2018).
- [26] M. Russ, D. M. Zajac, A. J. Sigillito, F. Borjans, J. M. Taylor, J. R. Petta, and G. Burkard, *Phys. Rev. B* **97**, 085421 (2018).
- [27] U. Güngördü and J. Kestner, APS March Meeting, Abstract:F28.00007 (2018).
- [28] C.-H. Huang and H.-S. Goan, *Phys. Rev. A* **95**, 062325 (2017).
- [29] See the supplementary material.
- [30] E. Milotti, *Phys. Rev. E* **51**, 3087 (1995).
- [31] J. P. Gleeson, *Phys. Rev. E* **72**, 011106 (2005).
- [32] S. L. Miller and D. Childers, *Probability and Random Processes with applications to signal processing and communications* (Academic Press, Boston, 2012).
- [33] R. L. Kosut, M. D. Grace, and C. Brif, *Phys. Rev. A* **88**, 052326 (2013).
- [34] L. S. Theis, F. Motzoi, and F. K. Wilhelm, *Phys. Rev. A* **93**, 012324 (2016).
- [35] F. Motzoi, J. M. Gambetta, S. T. Merkel, and F. K. Wilhelm, *Phys. Rev. A* **84**, 022307 (2011).
- [36] T. Meunier, V. E. Calado, and L. M. K. Vandersypen, *Phys. Rev. B* **83**, 121403 (2011).
- [37] A. G. Fowler, M. Mariantoni, J. M. Martinis, and A. N. Cleland, *Phys. Rev. A* **86**, 032324 (2012).

**SUPPLEMENTARY MATERIAL FOR “HIGH-FIDELITY AND ROBUST TWO-QUBIT GATES FOR QUANTUM-DOT SPIN QUBITS IN SILICON”**

**I. GATE INFIDELITY CONTRIBUTION FROM SINGLE-QUBIT DEPHASING NOISE**

We evaluate the gate infidelity contributed from the residual single-qubit decoherence. The dephasing noise spectrum of the  $^{31}\text{P}$  electron spin qubit in the isotopically enriched silicon was measured to be  $S(\omega) \propto 1/f^{2.5} + c$  in the frequency range of  $10^3 - 10^5\text{Hz}$ , where  $c$  is a constant and the plausible sources of the low-frequency noise could be thermal noise and magnetic noise due to the instability of the external magnetic field [1]. Here we use the same form of noise spectrum for our quantum-dot spin qubits as they both are in the same isotopically enriched  $^{28}\text{Si}$  substrate. For the quantum-dot electron spin qubit in the GaAs substrate, the dephasing noise spectrum  $\sim 1/f^{2.6}$  in the frequency range of  $10^1 - 10^5\text{Hz}$  has also been observed [2]. To extract the correct noise strength for our target silicon quantum-dot system [3], we use an ensemble of the dephasing noise realizations for different average noise standard deviations to simulate the decay of the single-qubit Ramsey fringe oscillations in Ref. [4] with the formula  $\frac{1}{2} + \frac{1}{2} \exp(-t/T_2^*)^n$  to find the best fitting result for the  $T_2^* = 120\mu\text{s}$  and  $n = 2$  [1]. The contribution to the ensemble average infidelity of our fine-tuned optimal CNOT gate from two independent dephasing noises on the two quantum dots with the obtained fitted noise strengths is  $\sim 3.43 \times 10^{-6}$ , which is around one order of magnitude smaller than  $\langle \mathcal{I} \rangle \cong 2.84 \times 10^{-5}$  obtained from the simulation for the electrical noise of  $\sigma_{U-\epsilon} = 2.4\text{GHz}$ . Therefore, the residual single-qubit dephasing noise in our target system does not affect the performance of the fine-tuned optimal CNOT gate demonstrated above. Besides, the contribution of the dephasing noise to the ensemble average infidelity of the ideal C-phase gate constructed without considering any noise effect is  $\sim 2.19 \times 10^{-5}$ , one order of magnitude larger than that of our CNOT gate. This shows that our optimal pulses have the ability to also suppress the dephasing noise even though we do not include the dephasing noise contribution into our total cost function for optimization.

**II. EFFECTIVE HAMILTONIAN FOR OPTIMIZATION**

Here, we explain in more detail how we obtain the effective Hamiltonian for optimization calculations. The values of the system parameters used in our Hamiltonian vary quite a lot:  $\bar{E}_Z = 39.16\text{GHz}$ ,  $\delta E_Z = -40\text{MHz}$ ,  $t_0 = 900\text{MHz}$ , and  $U - \epsilon = 276.71\text{GHz}$ . The largest value in these parameters is over 6900 times greater than the smallest one. Thus to obtain the exact dynamics, one needs to choose much smaller time-step for computation i.e., requires very long computation time. For computation efficiency in our numerical optimization, we apply two approximations to the Hamiltonian: the first one is to use the Schrieffer-Wolff (SW) transformation [5] and keep terms up to the second order, and the other one is to apply the rotating-wave approximation (RWA). Once we obtain the optimal control pulses to suppress the gate error from the noise, we will input the control pulses to the full Hamiltonian without using these approximations to calculate the gate infidelity.

Using the SW transformation, we transform the ideal Hamiltonian  $\mathcal{H}_I(t)$  to

$$\tilde{\mathcal{H}}_I^{\text{SW}}(t) = e^S \mathcal{H}_I(t) e^{-S}, \quad (\text{S-5})$$

where

$$S = \begin{pmatrix} 0 & 0 & 0 & 0 & 0 \\ 0 & 0 & 0 & 0 & -\gamma(-\delta E_Z) \\ 0 & 0 & 0 & 0 & \gamma(\delta E_Z) \\ 0 & 0 & 0 & 0 & 0 \\ 0 & \gamma(-\delta E_Z) & -\gamma(\delta E_Z) & 0 & 0 \end{pmatrix}, \quad (\text{S-6})$$

and

$$\gamma(\delta E_Z) = \frac{t_0}{U - \epsilon + \delta E_Z/2}. \quad (\text{S-7})$$

For  $(U - \epsilon) \gg t_0$  and  $(U - \epsilon) \gg |\delta E_Z|$ , we can expand  $\tilde{\mathcal{H}}_I^{\text{SW}}(t)$  in Eq. (S-5) to the second order of  $S$  and omit the

terms including  $O[\gamma^2(\delta E_Z)]$  or  $[\gamma(-\delta E_Z) - \gamma(\delta E_Z)]$  to obtain the Hamiltonian

$$\tilde{\mathcal{H}}_I^{\text{SWA}}(t) = \begin{pmatrix} 0 & & & & \\ & \tilde{\mathcal{H}}_{I,4 \times 4}^{\text{SWA}}(t) & & & \\ & & 0 & & \\ & & & 0 & \\ & & & & 0 \\ 0 & 0 & 0 & 0 & \tilde{\mathcal{H}}_I^{\text{SWA}}(5,5) \end{pmatrix}, \quad (\text{S-8})$$

where

$$\tilde{\mathcal{H}}_{I,4 \times 4}^{\text{SWA}}(t) = h \begin{pmatrix} \bar{E}_Z & \frac{1}{2}E_X(t) & \frac{1}{2}E_X(t) & 0 \\ \frac{1}{2}E_X(t) & \frac{1}{2}\delta E_Z - J_m & \frac{1}{2}(J_p + J_m) & \frac{1}{2}E_X(t) \\ \frac{1}{2}E_X(t) & \frac{1}{2}(J_p + J_m) & -\frac{1}{2}\delta E_Z - J_m & \frac{1}{2}E_X(t) \\ 0 & \frac{1}{2}E_X(t) & \frac{1}{2}E_X(t) & -\bar{E}_Z \end{pmatrix}, \quad (\text{S-9})$$

$\tilde{\mathcal{H}}_I^{\text{SWA}}(5,5) = U - \epsilon + J_p + J_m$ , and

$$J_p \equiv \frac{t_0^2}{U - \epsilon + \delta E_Z/2}, \quad (\text{S-10})$$

$$J_m \equiv \frac{t_0^2}{U - \epsilon - \delta E_Z/2}. \quad (\text{S-11})$$

The superscripts SWA denote the Hamiltonian with the above approximation after the Schrieffer-Wolff transformation. The elements of the Hamiltonian  $\tilde{\mathcal{H}}_I^{\text{SWA}}(t)$  in the subspace spanned by the computational basis states  $\{|\uparrow, \uparrow\rangle, |\uparrow, \downarrow\rangle, |\downarrow, \uparrow\rangle, |\downarrow, \downarrow\rangle\}$  and in the subspace of  $|0, 2\rangle$  are decoupled. Therefore, we can simulate the dynamics of the system in the above two subspaces separately.

Since the strengths of the control pulses  $|\Omega_X(t)|$  and  $|\Omega_Y(t)|$  are constrained to be smaller than 1mT, the maximum value of  $\frac{1}{2}|E_X(t)|$  is at most  $\sim 28\text{MHz}$ , which is over 1000 times smaller than  $\bar{E}_Z = 39.16\text{GHz}$ . Thus, we can apply the RWA to the Hamiltonian. Transforming  $\tilde{\mathcal{H}}_{I,4 \times 4}^{\text{SWA}}(t)$  to the rotating frame (RF), we obtain the Hamiltonian in the computational state basis as

$$\tilde{\mathcal{H}}_{I,4 \times 4}^{\text{SWA,RF}}(t) = U_0^\dagger(t)\tilde{\mathcal{H}}_{I,4 \times 4}^{\text{SWA}}(t)U_0(t) - i\hbar U_0^\dagger(t)\dot{U}_0(t), \quad (\text{S-12})$$

where

$$U_0(t) = \begin{pmatrix} \exp(-i\bar{E}_Z 2\pi t) & 0 & 0 & 0 \\ 0 & 10 & 0 & 0 \\ 0 & 01 & 0 & 0 \\ 0 & 0 & 0 & \exp(+i\bar{E}_Z 2\pi t) \end{pmatrix}. \quad (\text{S-13})$$

Then, by making the RWA, Eq. (S-12) becomes

$$\begin{aligned} & \tilde{\mathcal{H}}_{I,4 \times 4}^{\text{SWA,RWA}}(t) \\ &= h \begin{pmatrix} 0 & \frac{1}{4}\bar{\Omega}_X(t) - i\frac{1}{4}\bar{\Omega}_Y(t) & \frac{1}{4}\bar{\Omega}_X(t) - i\frac{1}{4}\bar{\Omega}_Y(t) & 0 \\ \frac{1}{4}\bar{\Omega}_X(t) + i\frac{1}{4}\bar{\Omega}_Y(t) & \frac{1}{2}\delta E_Z - J_m & \frac{1}{2}(J_p + J_m) & \frac{1}{4}\bar{\Omega}_X(t) - i\frac{1}{4}\bar{\Omega}_Y(t) \\ \frac{1}{4}\bar{\Omega}_X(t) + i\frac{1}{4}\bar{\Omega}_Y(t) & \frac{1}{2}(J_p + J_m) & -\frac{1}{2}\delta E_Z - J_m & \frac{1}{4}\bar{\Omega}_X(t) - i\frac{1}{4}\bar{\Omega}_Y(t) \\ 0 & \frac{1}{4}\bar{\Omega}_X(t) + i\frac{1}{4}\bar{\Omega}_Y(t) & \frac{1}{4}\bar{\Omega}_X(t) + i\frac{1}{4}\bar{\Omega}_Y(t) & 0 \end{pmatrix}, \end{aligned} \quad (\text{S-14})$$

where  $\bar{\Omega}_X(t) \equiv \frac{g\mu_B}{h}\Omega_X(t)$  and  $\bar{\Omega}_Y(t) \equiv \frac{g\mu_B}{h}\Omega_Y(t)$ . After the above two approximations (SWA and RWA), the parameters in the Hamiltonian  $\tilde{\mathcal{H}}_{I,4 \times 4}^{\text{SWA,RWA}}(t)$  range only from  $\sim 2.9\text{MHz}$  to  $40\text{MHz}$ , and thus we can save a lot of computation time to obtain the propagator  $\tilde{U}_{I,4 \times 4}^{\text{SWA,RWA}}(t)$  of the Hamiltonian  $\tilde{\mathcal{H}}_{I,4 \times 4}^{\text{SWA,RWA}}(t)$  by the Schrödinger equation. Then transforming this propagator  $\tilde{U}_{I,4 \times 4}^{\text{SWA,RWA}}(t)$  from the rotating frame back to the frame transformed by the SW transformation and combining it with the propagator in the subspace  $|0, 2\rangle$  in the same frame, we obtain the propagator in the full space

$$\tilde{U}_I^{\text{SWA}}(t) = \begin{pmatrix} 0 & & & & \\ & \tilde{U}_{I,4 \times 4}^{\text{SWA}}(t) & & & \\ & & 0 & & \\ & & & 0 & \\ & & & & 0 \\ 0 & 0 & 0 & 0 & \exp(-i\{U - \epsilon + J_p + J_m\}2\pi t) \end{pmatrix}. \quad (\text{S-15})$$



Finally, the ideal system propagator in the original frame,  $U_I(t)$ , is obtained via the transformation

$$U_I(t) \cong e^{-S} \tilde{U}_I^{\text{SWA}}(t) e^{+S}, \quad (\text{S-16})$$

where we expand  $e^{-S}$  and  $e^{+S}$  to the second order of  $S$ . Finally, we substitute the propagator  $U_I(t)$  into the total cost function  $\mathcal{K}$  of Eq. (6) of the main text for optimization to find the control pulses. However, to calculate the performance of our gates, we apply the obtained optimal control pulses to the full realistic Hamiltonian  $\mathcal{H}(t)$  of Eq. (3) of the main text without these approximations to simulate the ensemble average infidelity  $\langle \mathcal{I} \rangle$  with an ensemble of one thousand noise realizations.

- [1] J. T. Muhonen, J. P. Dehollain, A. Laucht, F. E. Hudson, R. Kalra, T. Sekiguchi, K. M. Itoh, D. N. Jamieson, J. C. McCallum, A. S. Dzurak, and A. Morello, *Nat Nano* 9, 986 (2014).
- [2] J. Medford, L. Cywiński, C. Barthel, C. M. Marcus, M. P. Hanson, and A. C. Gossard, *Phys. Rev. Lett.* 108, 086802 (2012).
- [3] M. Veldhorst, C. H. Yang, J. C. C. Hwang, W. Huang, J. P. Dehollain, J. T. Muhonen, S. Simmons, A. Laucht, F. E. Hudson, K. M. Itoh, A. Morello, and A. S. Dzurak, *Nature* 526, 410 (2015).
- [4] M. Veldhorst, J. C. C. Hwang, C. H. Yang, A. W. Leenstra, B. de Ronde, J. P. Dehollain, J. T. Muhonen, F. E. Hudson, K. M. Itoh, A. Morello, and A. S. Dzurak, *Nat. Nanotech.* 9, 981 (2014).
- [5] T. Meunier, V. E. Calado, and L. M. K. Vandersypen, *Phys. Rev. B* 83, 121403 (2011).